Surface & Coatings Technology 214 (2013) 19–29

Contents lists available at SciVerse ScienceDirect

Surface & Coatings Technology

journal homepage: www.elsevier.com/locate/surfcoat

Effect of processing parameters on titanium nitrided surface layers produced by laser gas nitriding

J.H. Abboud *

Mechanical Engineering Department, Faculty of Engineering, University of Benghazi (previously Garyounis), P.O. Box 1308, Benghazi, Libya

ARTICLE INFO

Article history:
Received 6 January 2012
Accepted in revised form 25 October 2012
Available online 3 November 2012

Keywords:
Titanium
Laser melting
Titanium nitride
Solidification

ABSTRACT

Experimental investigations based on Response Surface Method (RSM) were carried out to study the influence of laser power, nitrogen flow rate, and scanning speed on the microstructure, depth, hardness, and cracking of a set of titanium nitrided surface layers produced by laser gas nitriding. Laser powers ranged between 1 and 5 kW, scanning speeds 5 to 20 mm/min, and nitrogen gas flow rate ranged from 500 to 4000 l/min. The aim was to use RSM in the design of experiment to find suitable processing parameters which produce deep and crack free nitrided layers with a high surface hardness. Optical microscope, scanning electron microscope equipped with energy dispersive spectroscopy (EDS) analysis, and X-ray diffraction were used to characterize the microstructure and composition of the nitrided layers. Microhardness at a distance of 0.15 mm from the surface for all tracks was measured. The results showed that laser melting of titanium surface in a nitrogen containing atmosphere has led to the formation of a nitrided layer characterized with a strong convective flow and of a dense structure of TiN dendrites heterogeneously distributed. The TiN dendrites, which formed either directly from the melt or as a result of the peritectic reaction $L + \alpha Ti \rightarrow TiN$, were of various sizes and shapes and distributed non uniformly. The volume fraction of TiN dendrites in the melted zone is a function of processing speed and power being higher at slower speed and high power. The convectional flow not only affects the surface quality but also leads to effective nitrogen transport to a deeper region. The formation of TiN significantly increases the microhardness of the surface but it makes the surface rough. The optimum process parameter settings which were determined statistically in terms of power, scanning speed and nitrogen gas flow rate were found to be 2.8 kW laser power, 5 mm/s scanning speed and 2000 l/h nitrogen flow rate which would result in a maximum microhardness of approximately 1900 $HV_{0.15}$.

1. Introduction

Titanium and titanium alloys possess several interesting features including high corrosion resistance, high strength-to-weight ratio, light weight, and the ability to maintain their properties at high temperatures. Because of these attractive properties, there has been increasing interest in recent years in using titanium and its alloys in many fields such as automotive, medical and aerospace engineering [1]. However, the low wear resistance and poor tribological behavior of the titanium and its alloys restrict the utilization in industrial applications which involve intensive wear. Therefore, there is an increasing interest for improving surface properties through various surface modification techniques. The formation of TiN on the surface of titanium and its alloys is a popular way to improve their wear and corrosion performance [2]. Solid state nitriding by chemical vapor deposition (CVD), plasma nitriding and physical vapor deposition (PVD) can be used for this purpose. However, all of these methods have their own drawbacks, such as the need of the whole workpiece to be heated, or that the coatings which are formed on the whole surface are brittle [2]. Another disadvantage is that the depth of the coatings or the hardened layer is restricted by the diffusivity of the nitrogen into the substrate. The previous drawbacks can be tackled by nitriding the titanium surface in the molten state using laser technology which is termed as Laser Gas Nitriding (LGN).

LGN of titanium alloys, which was initiated by Katayama et al. in 1983 [3] and extensively continue by considerable research studies [3–33], involves the feeding of nitrogen gas into the melted pool generated by the laser beam in which TiN particles precipitate during solidification. Most methods of producing LGN surfaces have used continuous wave (CW) lasers but there are a few studies using pulsed lasers. Recently, TiN coatings were generated for the first time by means of a free electron laser (FEL) [4]. An excellent reviewing paper about laser nitriding was made by Höche and Schaaf [5] who reported that the process utilizing laser contains many different processes like heat transport and melting affects, diffusion and convection which partially determine the synthesized coating. Convection not only affects the surface quality but also leads to effective nitrogen transport to a deeper region [6,7]. The results of the micro-structural assessments of the laser nitrided layer on commercial pure (CP) titanium and Ti–6Al–4V alloy showed fcc TiN dendrite

* Tel.: +218 914344073.
E-mail address: jhabboud@yahoo.com.

0257-8972/$ – see front matter © 2012 Elsevier B.V. All rights reserved.
http://dx.doi.org/10.1016/j.surfcoat.2012.10.059

Table 1
The ranges of the laser nitriding parameters.

Factors	Power (P) kW	Speed (V) mm/s	Flow rate (q) l/h
Low level	1	5	500
High level	5	20	4000

at the top layer and a mixture of TiN and needles of hcp α′-Ti in the lower zone [8–22,31]. The TiN dendrites have a very effective role in increasing the hardness and the larger volume fraction of the TiN dendrites formed the higher the hardness of the resulting layer [9,10,12,21]. The high level of hardness obtained (more than 1000 HV as compared to 200 HV which is the hardness of the CP Ti) and the improvements of tribological properties have made the technique of LGN an effective and feasible method for surface hardening of a local area of the titanium alloys which cannot be hardened by conventional method. Furthermore, these nitride layers are usually non-reactive, which leads to an improvement in corrosion protection [23,24]. However, the fatigue strength was reduced because of the microcracks which formed during solidification [31].

The effect of different laser powers on the resulting microstructure and microhardness was studied by Yilbas et al. [27]. They employed CO_2 laser gas nitriding on Ti-64 alloys at two different laser powers. They reported that δ-TiN and ε-TiN were dominant at the surface of the treated alloy. More importantly, cracks were observed at high laser powers where there is a high concentration of nitrogen. In another work [28], the effect of gas flow rates, in laser gas nitriding samples of Ti–6Al–4V, on the resulting microstructure and hardness values was investigated. It was found that the microstructure is composed of dendrites in which their concentration was found to increase as the gas flow rate and laser energy densities increase. The formation of TiN dendrites was examined along with the alloy matrix by Man et al. [29] after subjecting the Ti–6Al–4V alloy to laser nitriding. It was shown that the fraction of dendrite structure can be controlled by monitoring the nitrogen flow rate during the treatment procedures. Nakai et al. [30] conducted some work aiming at exploring the changes in microstructure of gas nitrided biomedical Ti alloys.

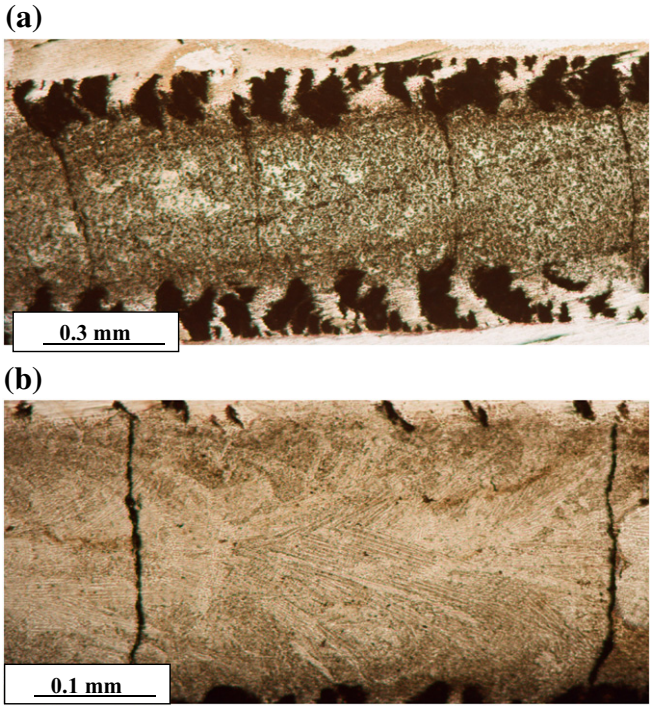

Fig. 1. (a and b): Optical micrograph showing the top section of the nitrided layer (3 kW, 12 mm/s, and 3125 l/h).

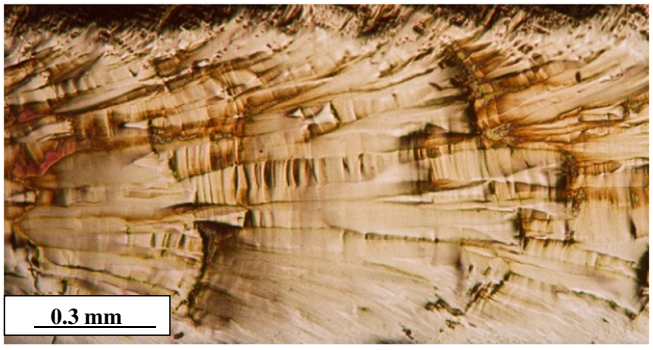

Fig. 2. Optical micrograph showing the top view of the laser nitrided layer after surface polishing.

They observed the presence of a TiO_2 layer at the surface of the alloy following the treatment. The competition between the formation of an oxide layer in addition to the presence of a nitrided layer resulted in its presence; nevertheless, significant improvement in hardness of the surface was observed by the presence of TiO_2. The effects of laser power, scanning speed and beam diameter on the TiN formation on a Ti–6Al–4V surface have been study by Jianglong et al. [32]. Their results showed that laser power density is the main factor for obtaining TiN and not laser interaction time. The power density should be greater than 5×10^4 W cm^{-2} in order to nitride the surface of Ti–6Al–4V in the presence of nitrogen gas.

Cracking is considered as one of the major problems associated with nitriding by laser. This defect, besides roughness and porosity, decreased dramatically the fatigue life of the components; microcracks act as metallurgical notches for fatigue failure. The development of crack-free TiN surface was achieved by diluting the nitrogen content for laser treated commercially pure titanium as reported by Mridha and Bakerce:[13], Abboud et al. [14], Weerasinghe et al. [15], and for Ti–6Al–4V alloy by Selamat et al.[16]. It was observed that controlling the processing parameters can yield a smooth, crack-free and deep nitrided layer with considerable improvement in hardness. Additionally, low scanning speed coupled with higher laser power can result in crack formation. However, this proved to be at the expense of both a lower hardness and a shallower melt depth. Preheating of the substrate is suggested by Hu and Baker [22] and via this process the crack formation at the surface is minimized.

LGN of titanium is influenced by several parameters which in some case reaches more than 30 parameters; some of them related to the laser type, beam diameter, beam mode, etc. while others related to the experimental arrangements such as traverse speed and working distance, nitrogen gas purity, pressure and flow rate. In order to optimize these parameters, a large number of experiments are required. In

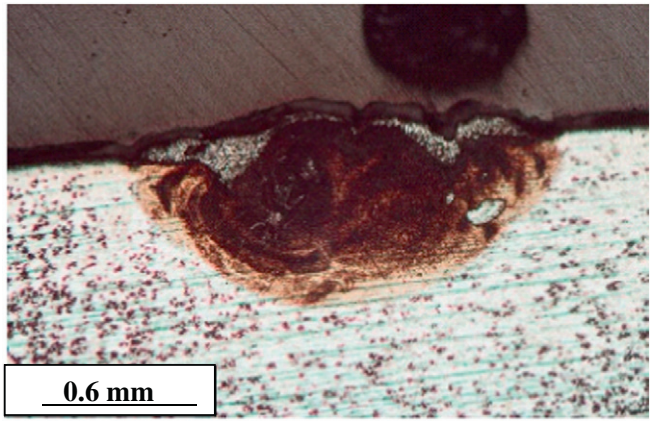

Fig. 3. Cross section of the nitrided layer produced at 500 l/h, 1 kW, 20 mm/s (sample 1).

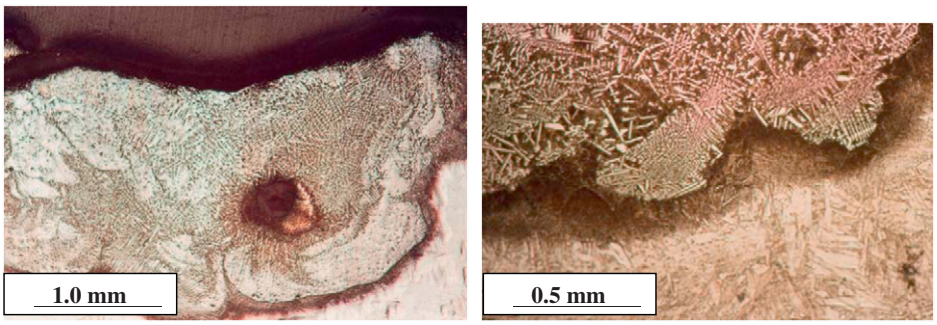

Fig. 4. Cross section of the nitrided layers produced at 500 l/h, 5 kW, 5 mm/s (sample 4).

this work, the effect of laser power, scanning speed, and flow rate of nitrogen gas on the nitride layer is investigated using design of experiment (DOE) statistical approach. Design of experiment (DOE) is a statistical method which is used to design the experimental work in a planned manner and to show the interaction effect between the various parameters considered. More specifically, Response Surface Method (RSM) in the design of experiment (DOE) has been utilized to perform the parametric studies, and to develop a statistical model which relates the independent variables of the nitriding process, with the performance variable response, and also to determine the optimum process setting to produce the maximum hardness.

Table 1 shows the design matrix factors considered and their high and low levels. These levels are estimated based on literature values and several trial experiments. After factor levels are determined the response surface design matrix is created using the MINITAB program [34].

2. Materials and methods

2.1. Materials and specimen preparation

Titanium plate of dimensions 100 mm × 100 mm × 8 mm supplied by Advent Research Materials Ltd was cut into sample pieces 10 mm × 20 mm × 8 mm using wire electric discharge machine (EDM). The purity of titanium is 99.6% and the other element is interstitial solid solution elements such as oxygen, nitrogen, and carbon.

Before laser nitriding, the surface of the titanium plate was abraded by emery papers (SiC) with grades from 80 to 320, and then cleaned ultrasonically with methanol.

2.2. Laser equipment

The laser machine used in this investigation is CO_2 laser operating in a continuous mode. The output power capacity is from 1 to 6 kW. The laser beam is Gaussian and focused by lens with a focal length of 200 mm. The distance between the focal point and the sample surface was kept constant at about 10 mm; this distance gives a beam diameter value ranged between 1 and 2 mm. For alignment procedure, a HeNe laser beam was transmitted along the optical axes. Nitrogen gas was introduced into the melted pool coaxially along the laser head and laterally through the shroud system which was attached with the laser head.

After the laser surface nitriding had been performed using the parameters in Table 1, the specimen was cut transversely to the direction of the laser track. The track cross-section was prepared, ground and polished. The polished specimens were chemically etched in a solution of 1% hydrofluoric acid in alcohol for a period of 10 s. After etching, the specimens were cleaned by alcohol and then dried by hot air. Microhardness was measured on transverse section and at a distance of 0.1 mm below the surface using a microhardness tester employing a load of 150 g. Optical microscopy, scanning electron microscopy equipped with EDS analysis and X-ray diffraction were used for microstructural analysis and phase identification. The X-ray diffraction was carried out using a high resolution Bruker Advance D8 XRD diffractometer in Bragg–Brentano geometry, with a CuKα monochromated beam ($\lambda = 0.15406$ Å) produced at 40 kV and 40 mA. The scanning electron microscope used in this experimental work was the 'EVO LS 15' developed by Carl Zeiss.

3. Results and discussion

3.1. Microstructure analysis

3.1.1. Top section

In the present work, it is found that most of the laser nitrided layers showed a golden color; some change from golden to gray or dark was observed specially in the samples processed at high power. The resulting nitrided surfaces are rough and contain many pores at the top edge of the nitrided layer (Fig. 1). Such pores were not seen when laser melting was performed in argon atmosphere [14]. In the present investigation, it was found that the number of pores is related to the processing parameters. Their number was high when a high

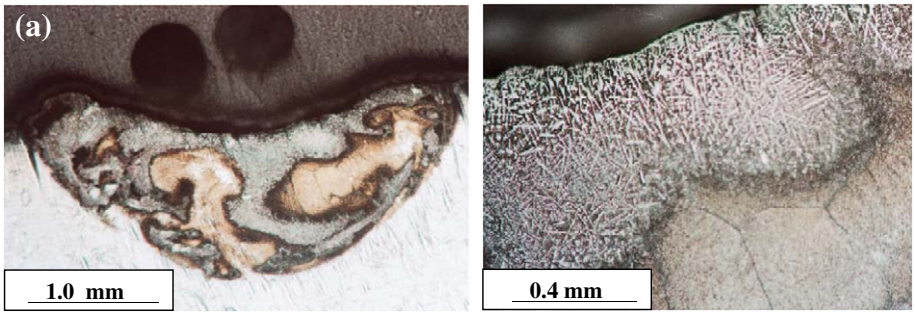

Fig. 5. Cross section of the nitrided layers produced at 500 l/h, 5 kW, and 20 mm/s (sample 5).

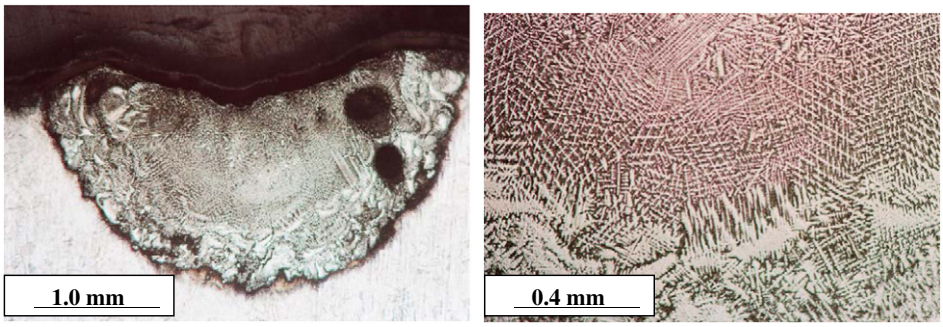

Fig. 6. Cross section of the laser nitrided layers produced at 2250 l/h, 2 kW, 12.5 mm/s (sample 15).

nitrogen gas flow rate and high power are used. Increasing the scanning speed reduces the number of these pores. The presence of pores at the edge of the melted pool has been attributed to the evolution of excess nitrogen gas from the solidifying melt pool. During surface melting in nitrogen environment, a large quantity of nitrogen gas entered into this shallow melt pool either by dissolution or bubbling. On solidification, the excess nitrogen in the liquid, which did not react with titanium, escaped via the surface of the melt pool. Because of the Gaussian energy distribution of the laser beam, the center region of the melt track attained higher temperature than the edges. As such the melt temperature at the edges was lower and on subsequent solidification the escaping gas left pores in these regions; the low viscosity of the melt near the edge was unable to fill up the pores, and thus produced porous regions. This explanation is supported in another investigation that showed an increase in the number of pore with increasing nitrogen flow rate [10]. Polishing the top surface without grinding revealed a combination of lamellae and ripples in radial direction (Fig. 2). These ripples represent the solidification fronts as they formed under the flow disturbance due to the surface tension gradient driven flow. As the freezing rate of the melt pool was relatively rapid, waves produced in the melt liquid would be frozen and formed ripples on the surface of the resolidified track, particularly noticeable at the track edges.

3.1.2. Transverse cross section

Cross sectional examination of all laser nitrided layers indicated that laser surface melting of commercial purity titanium in pure nitrogen produced a dendritic structure in the upper part of the melted pool and a mixture of dendrites and needle like structure in the lower part. This type of structure was observed under all the processing conditions. The volume fraction, concentration, distribution, and the scale of these dendrites are strongly dependent on the laser power and specimen speed and to a lesser extent to nitrogen flow rate. For example using the minimum values of flow rate (500 l/h), speed (20 mm/s) and power (1 kW) leads to a small melted pool with a dendritic structure concentrated mainly on the top surface (Fig. 3); the depths to which these dendrites extend did not exceed 10 to 20 μm. Using the same flow rate but with increasing the laser power and decreasing scanning speed (5 kW and 5 mm/s), the melted pool became deep with a high proportion of dendrites of various sizes extending deep into the lower part of the melted zone (Fig. 4). In this sample, the interface is irregular possibly as a result of the mushy zone created by the formation of TiN dendrites in the melt pool and the excess heat resulted from the exothermic reaction due to the formation of TiN phase; such interface was not seen in the sample surface melted without nitrogen gas (with argon gas, see Ref. [14]). However, this combination of high power and slow speed has led to the formation of a pore and made the surface rough. Increasing specimen speed to 20 mm/s and keeping power and flow rate without change (500 l/h, 5 kW), resulted in a melt pool partially nitrided (Fig. 5) with more than 50% of the melted pool free of nitrogen. Convectional flow of the melt due to surface tension gradient and hydrodynamic forces is very clear in this micrograph; this convective flow seems to play a significant role in determining the heterogeneity in the melted zone. Apparently at fast speed, the interaction time is too short to allow the nitrogen to diffuse into the whole zone leaving large area of the melted zone free of nitrogen.

Figs. 6 to 8 show transverse sections of melted pools produced at an intermediate range of flow rate (2250 l/h) but with different powers and speeds. It is very clear from these figures that increasing the flow rate leads to increases both the volume fraction of the dendrites and melted depth. The sharp increased of the melted depth in Fig. 8 could be explained on the exothermic reaction involving $L + N \rightarrow TiN + \text{heat}$. The nitride layer showed strong flow patterns in the melt zone with large dendrites accumulated along the flow lines (Fig. 8). However, in regions away from the convectional flow lines there were small dendrites, needles and basket-weave type structures (Fig. 6). In this set of nitrided layers there are dendrites of various sizes.

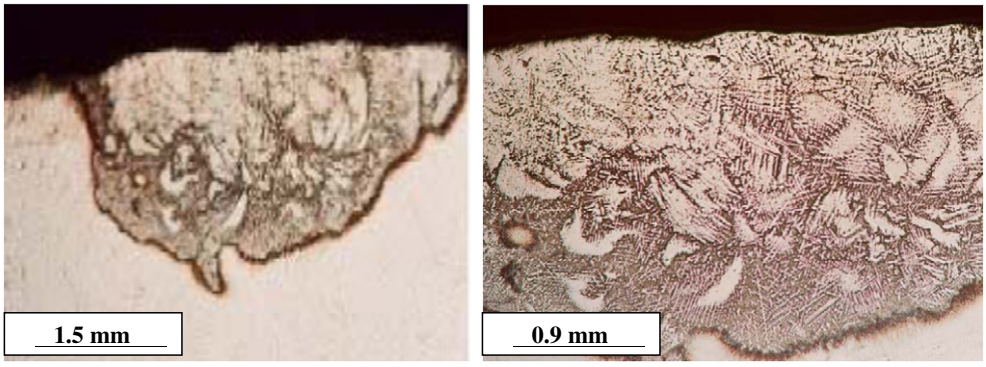

Fig. 7. Cross section of the nitrided layers produced at 2250 l/h, 3 kW, and 16.25 mm/s (sample 20).

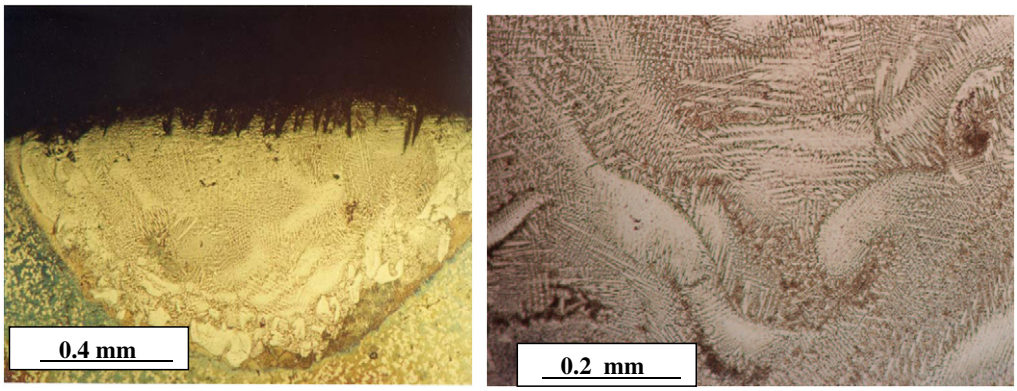

Fig. 8. Cross section of the nitrided layers produced at 2250 l/h, 3 kW, and 12.5 mm/s (sample 18).

Figs. 9 to 11 showed that increasing the flow rate beyond 2250 l/h and reaching maximum allowed flow rate (for example to 4000 l/h). At the maximum heat input and flow rate, the rippling became more severe with more convectional eddies (Fig. 9). These flow loops draw the nitrogen gas from the surface into the deeper melted zone and consequently increase the depth of the nitrided layer. The melt flow velocity induced by the Marangoni force has been calculated to be approximately 1 m/s [5]. This strong flow is also the governing process of the nitrogen transport. For deeper nitriding, it is necessary to increase the melting depth and the convectional flow, which leads to efficient nitrogen transport in deeper regions. On the other hand, this requires higher energy densities, which lead to large surface deformation because of strong capillary forces and a decrease in quality (roughness).

Generally, the microstructure of the melted pool under all processing conditions consisted of fine and coarse dendrites distributed through the melted pool. The distribution appeared to be inhomogeneous. Within a single melt pool, different TiN concentrations were observed. The differences in the sizes of the dendrites might be due to different temperatures within the melted pool leading to different rates of formation of dendrites. In some regions, large dendrites join to form a compact dendritic structure. Also, it has been shown that TiN dendrites did not grow from the top down direction as reported by previous authors [9,10,18,19]; this is due to the huge difference in solidification temperatures and the heat transfer conditions. The TiN develops on top of the melt pool and resolidification can even start at the Ti solid liquid interface in top direction.

In order to study the microstructure of the nitride layers and to carry out compositional analysis, a typical sample (sample 20) was selected for this purpose. Fig. 12a shows the dendritic structure in the upper part of the nitride layer. It consists of a massive dendrite and primary dendrites originating from the big one and secondary dendrites branching from the primary dendrites. The secondary arm spacing was about 2 μm indicating a high rate of cooling. The area between the dendrites showed small plates which might be precipitated during cooling. The lower part of the nitride layer showed a needle like structure. Fig 12b shows needle and platelet type particles below the dense dendrites near the surface. This type of structure presumably resulted from the fast cooling of the high temperature β phase to α′. Elemental analysis by energy dispersive spectroscopy (EDS) attached with the SEM showed that the nitrogen depth profile has a gradient feature (Fig. 12d). Nitrogen concentration was 30 at.% near the surface dropping to 16% in the lower part. This is due to the nitrogen diffusion rate, which becomes less as the distance from the surface increases. Point analysis was also performed on the same sample at the center of the melt pool and the results showed that the composition of the dendrites (the white phase) was 25 at.% (9 wt.%) while between the dendrites (the dark phase) it was 3.54 at.% (1%). According to the Ti–N phase diagram [35] which is shown in Fig. 13, the average composition of the layer lies in the two phase region namely, TiN and αTi and solidification of this nitride layer commences with primary TiN dendrites. Because of the high melting point of TiN (~3220 K), the TiN dendrites will form first at the surface of the pool. They will not necessarily solidify from the bottom or edges. The concentration of nitrogen in the melt will depend on time and temperature to allow diffusion (there is also considerable stirring due to Marangoni forces). Thus the nitrogen concentration is a function of processing speed being higher at slower speeds (see Figs. 7 to 9). The TiN which forms in the melt surface are free dendrite not attached to a wall or anything in particular and therefore will be washed around by the stirring action in the pool; clusters of dendrites will swirl around. As the number of dendrites increases (a function of time and therefore process speed) the flow will become stiffer in the pool which is becoming mushy. Finally solidification of the pool will take place making TiN + αTi. However the result will be a rough surface due to the preformed dendrites and the solidified mushy surface which was different from melting under argon.

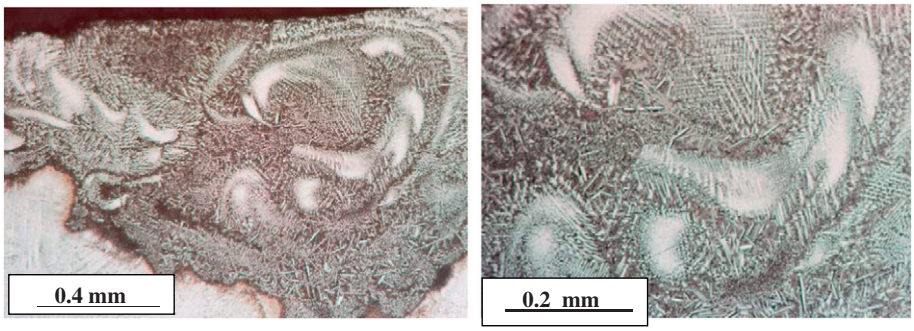

Fig. 9. Cross section of the nitrided layers produced at 4000 l/h, 5 kW, and 5 mm/s (sample 11).

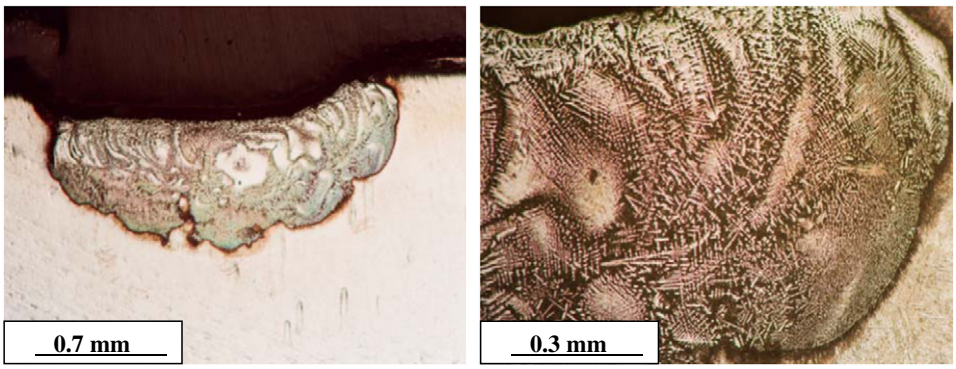

Fig. 10. Cross section of the laser nitrided layers processed at 4000 l/h, 5 kW, and 20 mm/s (sample 14).

The mechanism of TiN formation during laser melting in nitrogen containing atmosphere is reported by Labudovic [4]. It was reported that Labudovic indicates that the following reactions arise during the layer synthesis:

1. adsorption: $[Ti] + N_2 \rightarrow [Ti] + [N_2]$
2. dissociation: $[N_2] \rightarrow 2\ N$
3. diffusion: [N] (surface) → [N] (surface)
4. TiN-formation: $[Ti(N)] \rightarrow TiN + [Ti(N)]$
5. solidification: $[Ti(N)] \rightarrow TiN + \alpha\text{-}Ti(N)$.

Square brackets [] mean in liquid phase. This makes clear, which complex sequences going on during the process. It is shown that besides the TiN nitrogen dissolution in the pure hexagonal α-titanium also occurs. Nwobu et al. [33] assume that nitrogen is incorporated by convection into the liquid titanium and the melt reacts in an exothermal reaction.

Although the composition of the nitride layer of sample 20 showed a composition corresponding to TiN and αTi with different proportions, it is necessary to determine the phases present in this nitride layer. Fig. 14 shows an XRD spectrum taken from the top of the nitrided layers of samples 20 and 15. Both XRD patterns showed two distinct phases mainly cubic titanium nitride (TiN) with strong peak intensity at (200) and hexagonal alpha-titanium nitride with lattice parameters slightly different from pure titanium and this phase is closer to TiN solid solution ($TiN_{0.3}$). These results are consistent with the microstructure at the top layer which showed high concentration of dendrites. Mridha and Baker ce:cross-ref>/ce:cross-ref> reported that $TiN_{0.3}$ has a hexagonal structure with a = 2.9737 and c = 4.9717 Å which is similar to pure α-Ti having a hexagonal structure with a = 2.9511 and c = 4.6843 Å. In addition they showed that the lattice parameters of $TiN_{0.3}$ depended on composition. Mridha and Baker [13], Selamat et al. [16] and Hu et al. [37], showed the same results but the angles were slightly different. Table 3 showed the average lattice constant of TiN and also compared these values with the reported value in the literature (Table 4). In the same way lattice constants of TiN in both samples 15 and 20 are shown in Table 5. The values obtained were 4.206 Å for sample 20 and 4.1915 Å; both these values are lower than that usually reported for stoichiometric TiN which was 4.242 Å [37]. It is very interesting to see that the lattice constant of TiN depends on composition. The higher the amount of nitrogen the more the lattice constant. Comparing again these results it is shown that the TiN compound in sample 20 has more nitrogen than in sample 15. This indicates that the solubility of nitrogen in titanium increases as the laser power increased. Sample 20 was processed at higher power than sample 15 and this gives more nitrogen in the TiN phase. It has been reported that when the nitrogen concentration in TiN changes from 35 to 50 at.%, the lattice parameters increase from 4.215 to 4.242 Å [37]. Baker and coworkers have established a linear relationship between nitrogen concentration in the TiN and the lattice parameters of TiN [37]. The relation showed that the lattice parameters of TiN increased with increasing nitrogen concentration reaching a maximum value 4.24 Å at 50 at.% nitrogen and then decreased. By plotting 4.2 Å as a lattice constant obtained in this work, gives ~25% nitrogen concentration which is very close to Fig. 12d.

3.2. Performance results

Performance results of the laser nitriding on pure titanium in terms of the $HV_{0.15}$, depth of nitriding layers, and crack frequency were inserted into the RSM (Response Surface Methodology) design matrix as shown in Table 2. All hardness values were taken at a depth of 0.15 mm below the surface.

At the beginning both the crack frequency and the layer depth are discussed on the experimental measurement basis. Then the completed $HV_{0.15}$ design matrix is analyzed with Response Surface Regression routines in the MINITAB program and the analysis results are presented

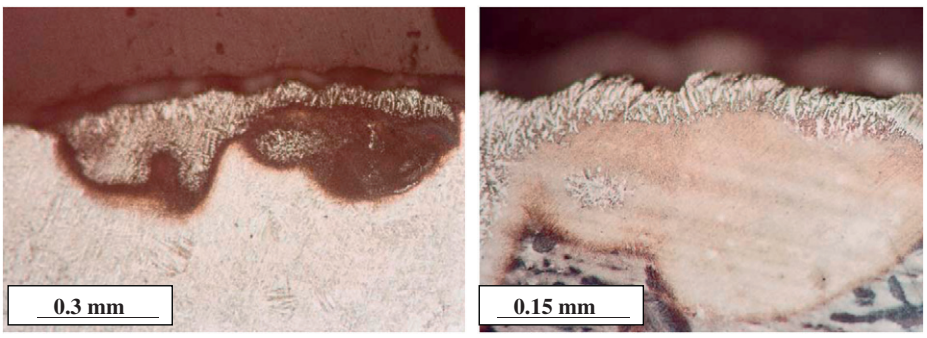

Fig. 11. Cross section of the nitrided layers processed at 4000 l/h, 1 kW, and 20 mm/s (sample 6).

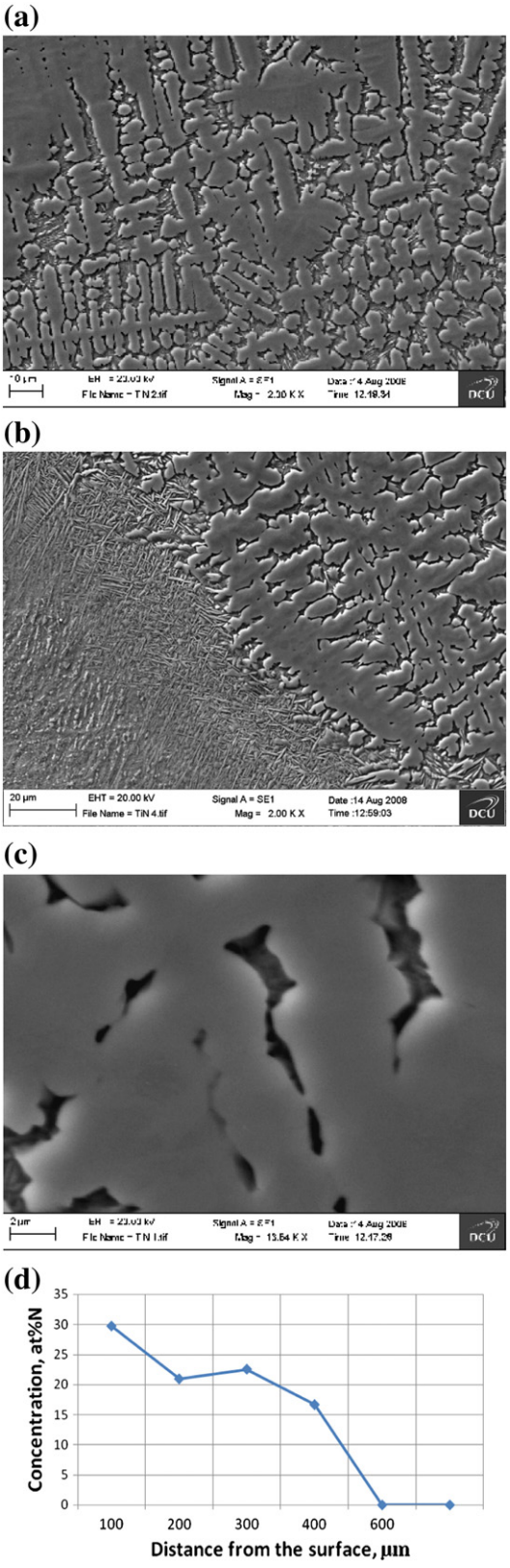

Fig. 12. (a–c): SEM micrographs taken from the nitrided layer processed at 2250 l/h, 3 kW, and 16.25 mm/s (sample 20), (d) compositional analysis across the nitride depth (sample 20: 3 kW, 16.25 mm/s, and 2250 l/h).

and discussed together with the multivariable model developed. This model is then utilized to produce the 3D surface plots which relate the titanium surface microhardness with the processing parameters and also to perform the microhardness optimization.

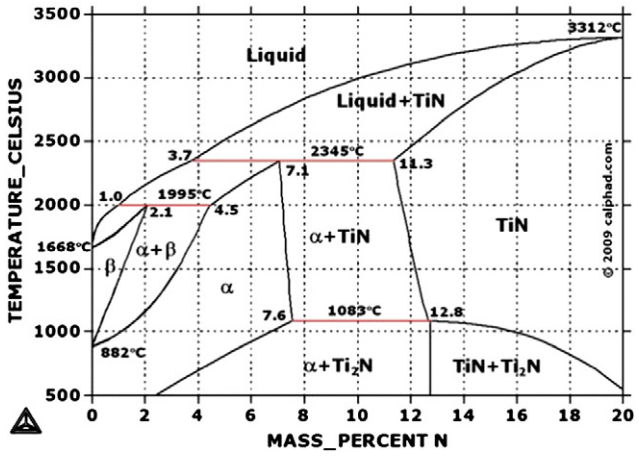

Fig. 13. TiN phase diagram.

3.2.1. Cracks

Generally, laser surface melting of material induces stress. The type of stress depends on several parameters including the ductility of the processed material and phase transformation that occur during rapid cooling. For ductile materials, these stresses could be relieved through plastic deformation. However, for brittle materials, the build-up of stresses may lead to cracking. In the present study and for a single track, no cracks were found parallel to the laser direction but when overlapping was performed, cracking in the center of the nitrided layer was seen. These cracks were formed due to buildup of stresses with each overlapping pass [36]. Examination of the top nitrided layers (see Fig. 1) showed cracks perpendicular to the laser direction across the width from one side to the other. The crack formation seems to occur at regular distances. A more probable explanation could be the stress energy stored in the shrinkage volume, which may have a critical value before cracking occurs. Plastic flow would be possible at the hot center but less likely at the chilled edges. Thus initiation is likely to start from the rough edges where there are regular stress raisers as seen in Fig 1.

Table 2 shows the relation between crack density (number of surface cracks per cm) and the different parameters used. It is apparent from the table that increasing the heat input (either by decreasing scanning speed or increasing laser power) tends to increase the crack intensity, while on the other hand, nitrided layers produced at low power (less than 1.5 kW) and fast speed (more than 20 mm/s) and low flow rate (less than 1000 l/h) did not show any cracks (see samples 1, 4, 6, and 15). While severe cracking was observed in the samples processed at high power and slow speed (see Table 2 samples 14 and 19), it has been shown that with high flow rate of nitrogen gas, the surplus nitrogen in liquid pool formed pores which ultimately initiated cracking. Also, the precipitation of TiN particles during cooling affects the viscosity of the melt. This result agreed partially with the results of Mridha and Baker [10] who showed that cracks were totally eliminated at fast speed (50 mm/s). Nitriding at fast speeds reduces the heat input in the melt pool; it also reduces the availability of nitrogen for interaction with liquid before it rapidly solidifies. Also, the greater the amount of nitride formation at high power and slow speed, the higher is the residual stress in the melt zone, and hence, an increased tendency for crack formation.

3.2.2. Nitrided layer depth

In the present investigation, the nitride layer depth, which was determined as the depth where the dendrites were terminated, was found to increase with increasing laser power and decreasing scanning speed. Increasing flow rate has a slight effect on the melted depth (see Table 2). The maximum melted depth obtained was 1.9 mm and

(a) X-ray diffraction pattern taken from the surface of nitride layers produced at 3kW, 16.25 mm/s, and 2250 l/h, (sample 20)

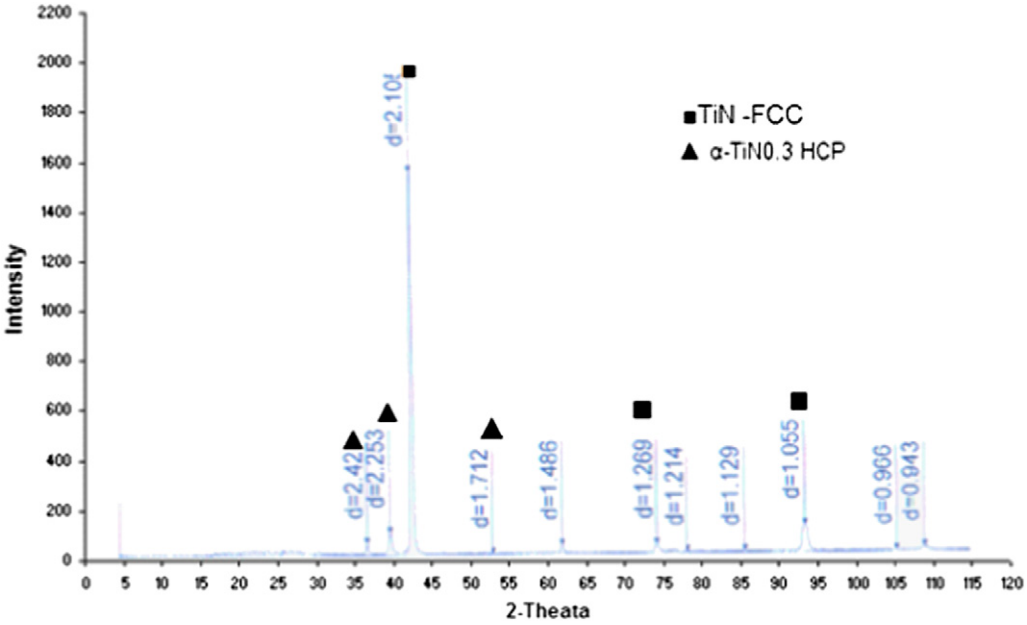

(b): X-ray diffraction patterns taken from the surface of nitride layerproduced at 2kW, 12.5 mm/s, 2250 l/h, (sample 15)

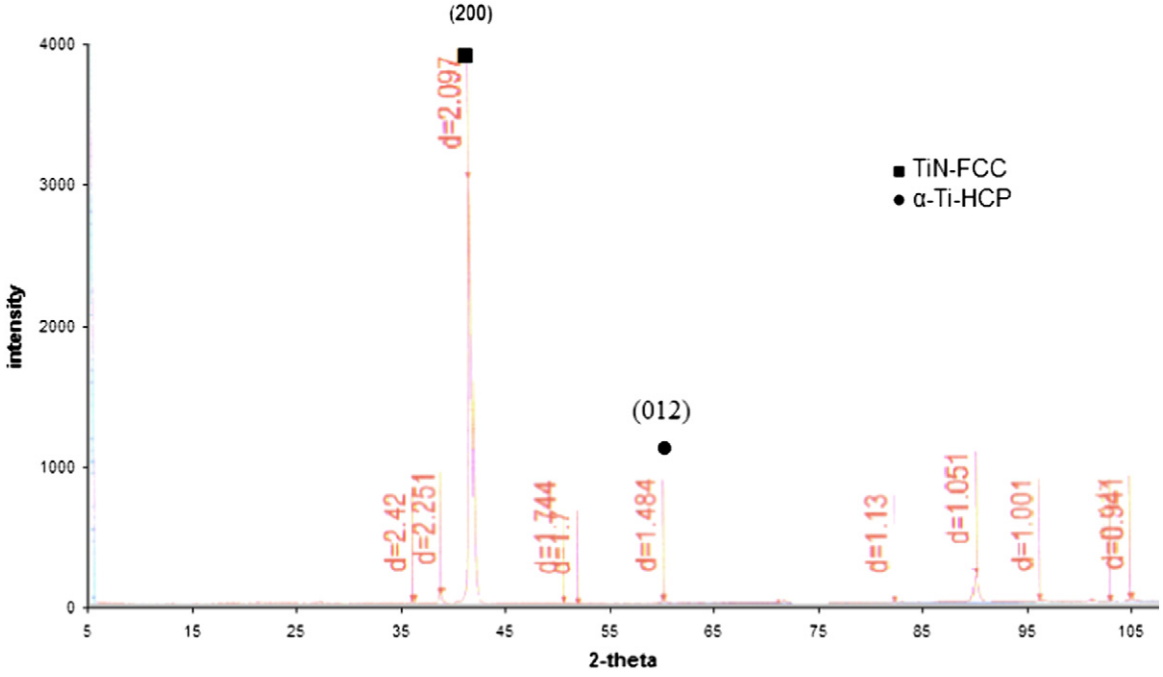

Fig. 14. (a) X-ray diffraction patterns taken from the surface of the nitrided layers produced at 3 kW, 16.25 mm/s, and 2250 l/h (sample 20), (b) X-ray diffraction patterns taken from the surface of the nitrided layer produced at 2 kW, 12.5 mm/s, and 2250 l/h (sample 15).

produced in the track processed at 3 kW, 12.5 mm/s, and 2250 l/h while the minimum melted zone produced at 1 kW, 20 mm/s, and 500 l/h has a melted depth of ~0.6 mm. This increase of the melted depth with increasing applied power is attributed to a high level of absorbed energy. Previous work [14] showed a linear relationship between decreasing speed and the increase of the melted depth while the relation between increasing laser power and the melted zone depth was nonlinear. Increasing laser power leads to an increase in the surface temperature; the higher laser power (or precisely the high power density) melts more material and gives a higher surface temperature. From the other side, at fast speeds the interaction time of the laser beam with the specimen surface is short to melt effectively and deeply,

Table 2
Laser nitriding response results.

Experiment no.	*Factors*			*Response*		
	q l/h	V mm/s	P kW	Microhardness $HV_{0.15}$	Depth mm	(No. of cracks/cm)
1	500	20	1	533	0.6	No crack
2	2250	12.5	4	1100	0.85	4
3	3125	12.5	3	988	1	3
4	500	5	5	788	1.34	No crack
5	500	20	5	625	0.93	5
6	4000	20	1	499	.320	No crack
7	2250	12.5	3	1097	0.78	5
8	2250	12.5	3	1200	1.2	5
9	2250	8.75	3	1300	1.55	2
10	2250	12.5	3	1235	1	5
11	4000	5	5	678	1.05	10
12	2250	12.5	3	1022	1.18	6
13	1375	12.5	3	1296	1.3	7
14	4000	20	5	600	0.65	9
15	2250	12.5	2	850	1.2	No crack
16	4000	5	1	1000	1.4	5
17	2250	12.5	3	990	1.26	4
18	2250	12.5	3	1263	1.07	8
19	500	5	1	1000	0.6	10
20	2250	16.25	3	1382	1.88	9

which leads finally to small nitride layer depth while at slow speeds, convective effects induce stresses and cracks and decrease the quality of the surface.

3.2.3. Microhardness

Table 2 shows the microhardness of the nitrided layers at depth of 0.15 mm below the surface for a range of processing parameters. This hardness value comprises both the TiN dendrites embedded in alpha titanium containing nitrogen in solution; this value despite very high, is less than the hardness of the pure TiN. All measurements present a strong increase in hardness with increasing TiN dendrites. The maximum hardness was 1384 HV obtained in the samples processed at intermediate values of power, speed and nitrogen flow rate. The increased of hardness is primarily due to the formation of TiN dendrites. The refinement of the microstructure and solid solution strengthening play another role in increasing the hardness. The higher hardness near the surface is directly related to the TiN dendrites.

In order to optimize hardness with respect to processing parameters, the RSM model is used to generate plots which relate the microhardness (response in this study) with the independent variables (factors) which are the power (P), scanning speed (V), and the nitrogen flow rate (q). To simplify interpreting the results, the effect of each factor will be considered as it exists separately and then the overall interpretation of the whole plot will be made.

Fig. 15 shows the 3D surface plot of the effects of power in kW and the speed in mm/s on the microhardness (Response) of the laser nitrided surface. By increasing the laser power the surface hardness increased. This hardness increase continues until the power reaches about 3 kW, where increasing the laser power further, the hardness starts decreasing. Therefore, according to this plot an optimum (maximum) microhardness setting is achieved with the laser power value around 3 kW.

Regarding the effect of the laser scanning speed as shown in Fig. 15 increasing the speed beyond the lower level of 5 mm/s the hardness had a decreasing trend. This decrease continued until reaching minimum microhardness at a scanning speed of approximately 12.5 mm/s, and then it starts increasing again until it reached to approximately the same starting point with a scanning speed of 20 mm/s.

Fig. 16 shows the 3D surface plot of the effects of power in kW and the flow rate in l/h on the surface microhardness. As shown from the 3D surface plot, by increasing the laser power, the surface hardness again increases until the microhardness reached approximately an optimum value when the power reached to about 3 kW. By increasing the laser power further, the hardness starts decreasing. This agrees very well with what is being found earlier from Fig. 15 and confirms that the optimum power setting is about 3 kW which will result in the maximum microhardness. Any setting higher than this value would have diverse effect on the microhardness besides it is considered as a wasted energy.

Regarding the flow rate it is clear from the 3D surface plot that increasing the flow rate increases (but not sharply) the microhardness until a certain level after which it starts to fall similar to the power trend.

Fig. 17 shows the 3D surface plot and contour plot of the effects of scanning speed in mm/s and the flow rate in l/h on the microhardness. It is evident that higher hardness values are obtained with lower and higher speeds (close to 5 and 20 mm/s). Furthermore, at flow rates close to 2000 l/h the highest hardness is obtained (see the 1800 $HV_{0.15}$ line). These findings are in agreement with previous findings and do not have any discrepancy which provides a further check on the results obtained from this work.

The results of Figs. 15 to 17 above have provided a comprehensive overview on the effect of the selected process parameters on the surface hardness of the laser nitrided titanium material. It seems that the optimum setting of the laser scanning power was sharply evident. However, the optimum settings of the flow rate and the speed could not be very well defined from these plots and therefore the maximum hardness setting as determined by the optimization chart will be required. This chart is produced by the response optimizer of the MINITAB program. The chart predicts that the optimum process parameter settings are 2.843 kW laser power, 5 mm/s scanning speed and 2076 l/h nitrogen flow rate which would result in a maximum predictable microhardness of 1920 $HV_{0.15}$. However, it needs to be remembered that this result is based on the response surface regression model and the actual measured value could be somewhat different. Therefore, it is very strongly suggested that this setting be implemented in the future and repeated a few times to confirm or

Table 3
d-Spacing, (hkl), and lattice parameters of the TiN phase for sample 20 at different Bragg's angles.

No.	2θ	d-Spacing Å	(hkl)	Lattice parameter Å
1	37.108	2.42	(111)	4.1915
2	42.916	2.105	(200)	4.210
3	62.423	1.486	(220)	4.203
4	74.719	1.269	(311)	4.2088
5	78.73	1.214	(222)	4.205
6	93.756	1.055	(400)	4.22
Average lattice parameters, Å				4.206

Table 4
Standard lattice constants of Ti, $TiN_{0.3}$ and TiN.

Phases	Structure	a, Å	c, Å
α-Ti	HCP	2.925	4.67
$TiN_{0.3}$	HCP	2.976	4.807
TiN	FCC	4.242	–

Table 5
Lattice constant of $TiN_{0.3}$ and TiN fcc in samples 20 and 15.

Sample no.	Parameters			Phases		
	P kW	V mm/s	q l/h	TiN	$TiN_{0.3}$	
				a Å	a Å	c Å
20	3	16.25	2250	4.206	2.985	4.790
15	2	12.5	2250	4.1915	2.98	4.810

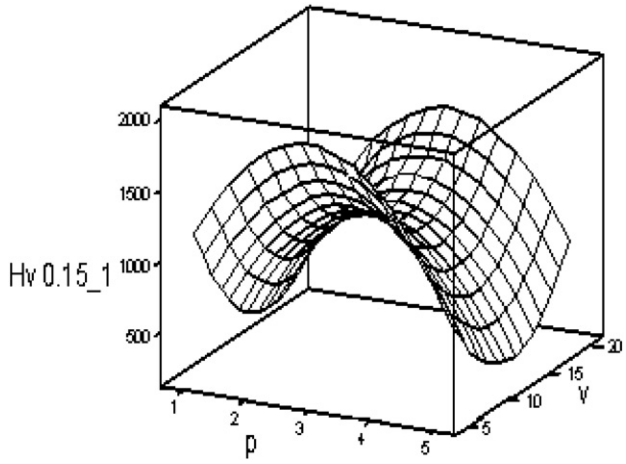

Fig. 15. 3D surface plot of the effects of power in kW and the speed in mm/s on the microhardness.

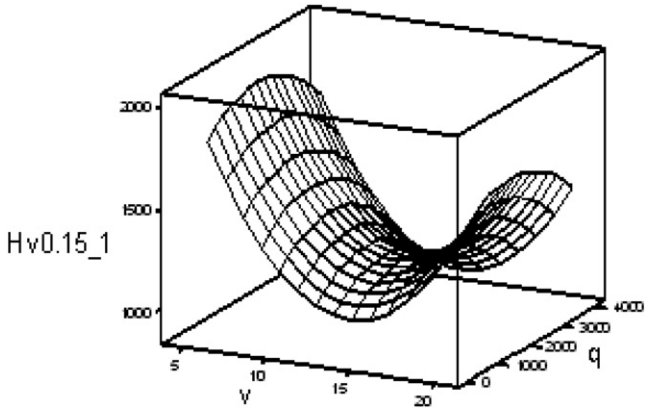

Fig. 17. 3D surface plot of the effects of scanning speed in mm/s and the flow rate in l/h on the microhardness.

otherwise refine the result. More specifically the effect of scanning speed needs to be investigated in depth with smaller ranges to have a final conclusion.

4. Conclusions

Laser surface melting of commercial pure titanium in nitrogen containing atmosphere has led to the formation of hard TiN dendrites embedded in soft titanium matrix. All the processing conditions used had led to the solidification of TiN. However, the volume fraction and distribution of TiN dendrites, their sizes and shapes depend greatly on laser power (or power density W/mm^2) and to a lesser extent to the specimen speed (or the interaction time between the specimen and the laser). The effect of flow rate seems to be the least affected parameter. Marangoni flow generates vortices in the melt pool that seem to have a considerable role in nitrogen diffusion into the depth of the melted pool especially for the samples processed at slow speeds and high powers. This flow appears to be seriously inhibited by the change of viscosity due to the formation of TiN dendrites in the melt due to the peritectic solidification so the melt pool thus becomes "mushy". The TiN dendrites which formed either directly or indirectly by the peritectic reaction $L+\alpha Ti \rightarrow TiN$ have a gradient feature and are heterogeneously distributed in the melted pool, partly due to the flow in the pool and partly due to gravity separating the lighter dendrites from the melt. The hardness increased with increasing the volume fraction of the TiN dendrites. Transverse cracks were observed in the nitrided layers produced at high powers and slow traverse speeds. A suitable combination of laser power (3–5 kW) and a relatively slow speed (7–15 mm/s) has been found to produce deep and hard nitride layer with many cracks. However crack free nitride layers were obtained at fast speed (more than 20 mm/s) and low power (less than 3 kW) but these conditions produced nitride layer of low hardness. Statistical analysis based on RSM has predicted a maximum hardness of about 1900 $HV_{0.15}$ if laser power, scanning speed, and nitrogen gas flow rate were 2.9 kW, 5 mm/s and 1800.5 l/h respectively.

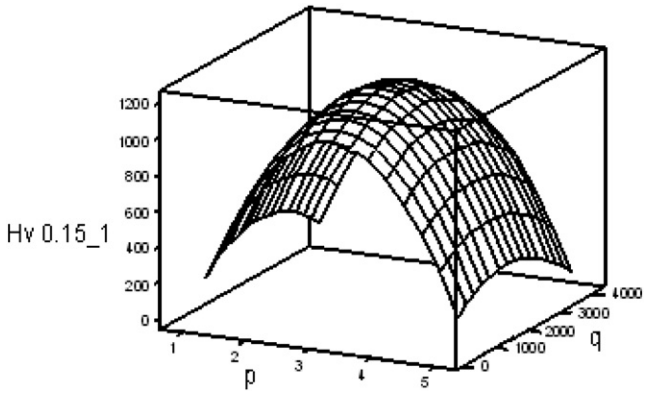

Fig. 16. 3D surface plot of the effects of power in kW and the flow rate in l/h on the surface microhardness.

Acknowledgments

The author appreciates the kind assistance and collaboration of the Welding Research Center in Tripoli, Libya, for allowing the use of the CO_2 laser, and also special thanks to professor William Steen at Liverpool University for his valuable comments.

References

[1] J. Polmear, Light Alloys, Edward Arnold, London, 1981.
[2] A. Zhercheva, W. Sha, S. Malinova, A. Long, Surf. Coat. Technol. 200 (2005) 2192.
[3] S. Katayama, A. Matsunawa, A. Morimoto, in: A. Metzbower (Ed.), Proceeding of Material Processing Symposium, vol. 38, Laser Institute of America, Naval Research Dept., Washington DC, 1983, p. 127.
[4] M. Labudovic, R. Kovacevic, I. Kmecko, T. Khan, D. Blecic, Z. Blecic, Metall. Mater. Trans. A 30 (1999) 1597.
[5] D. Höche, Peter Schaaf, Heat Mass Transfer 47 (2011) 519.
[6] D. Höche, M. Shinn, J. Kaspar, G. Rapin, P. Schaaf, J. Phys. D Appl. Phys. 40 (2007) 818.
[7] D. Höche, Sven Mu, Ller Gerd Rapin, Michelle Shinn, Elvira Remdt, Maik Gubisch, Peter Schaaf, Metall. Mater. Trans. B 40 (2009) 499.
[8] T. Bell, H.W. Bergmann, J. Lanagan, P.H. Morton, A.M. Staines, Surf. Eng. 2 (1986) 133.
[9] S. Mridha, T.N. Baker, Mater. Sci. Eng. A142 (1991) 115.
[10] S. Mridha, T.N. Baker, J. Mater. Process. Technol. 77 (1998) 115.
[11] P. Jiang, L. Hex, X.X. Li, G. Yu L, H.M. Wang, Surf. Coat. Technol. 130 (2000) 24.
[12] A. Biswas, L. Li, U.K. Chatterjee, I. Manna, J. Dutta Majumdar, Metall. Mater. Trans. A 40 (2009) 3031.
[13] S. Mridha, T.N. Baker, Mater. Sci. Eng. 188 (1994) 229.
[14] J.H. Abboud, A.F. Fidel, K.Y. Benyounis, Opt. Laser Technol. 40 (2008) 405.
[15] V.M. Weerasinghe, D.R.F. West, M. Czajlik, in: 1st ASM conf. on Heat Treatment and Surf. Eng., Amsterdam, 1991.
[16] M.S. Selamat, T.N. Baker, L.M. Watson, J. Mater. Process. Technol. 113 (2001) 509.
[17] Z. Sun, I. Annergren, D. Pan, A. Mai, Mater. Sci. Eng., A 345 (2003) 293.
[18] H. Xin, S. Mridha, T.N. Baker, J. Mater. Sci. 31 (1996) 22.
[19] A. Walker, J. Folkes, W.M. Steen, D.R.F. West, Surf. Eng. 1 (1985) 23.
[20] M.S.F. Lima, F. Folio, S. Mischler, Surf. Coat. Technol. 199 (2005) 83.
[21] A.B. Klosterman, J.T.M. De Hosson, Scr. Metall. Mater. 33 (4) (1995) 567.
[22] C. Hu, T.N. Baker, Mater. Sci. Eng. A 265 (1999) 268.
[23] V.M. Weerasinghe, D.R.F. West, J. de Damborenea, J. Mater. Process. Technol. 58 (1996) 79.
[24] B.S. Yilbas, A.Z. Sahin, Z. Ahmad, B.A. Abdulaleem, Corros. Sci. 37 (1995) 1627.
[25] C. Gerdes, A. Karimi, H.W. Bieler, in: Wear 186–187, 1995, p. 368.
[26] B. Courant, J.J. Hantzpergue, S. Benayoun, Wear 236 (1999) 39.
[27] B.S. Yilbas, C. Karatas, Uslan, O. Keles, I. Usta, M. Ahsan, Appl. Surf. Sci. 252 (2006) 8557.
[28] J. Kaspar, J. Bretschneide, S. Jacob, S. Bonß, B. Winderlich, B. Brenner, Surf. Engg. 23 (2007) 99.

[29] H. Man, N. Zhao, Z. Cui, Surf. Coat. Technol. 192 (2005) 341.
[30] M. Nakai, M. Niinomi, T. Akahori, N. Ohtsu, H. Nishimura, H. Toda, H. Fukui, M. Ogawa, Mater. Sci. Eng., A 486 (2008) 193.
[31] B.L. Mordike, in: Series E: Applied Sciences, no. 115 NATO ASI Series 389, 1986.
[32] Liu Jainglong, Luo Qiquan, Zou zhirong, Surf. Coat. Technol. 57 (1993) 191.
[33] A.I. Nwobu, R.D. Rawlings, D.R.F. West, Acta Mater. 47 (1999) 631.
[34] MINITAB User Guide, Version 13, 2002. (USA).
[35] J.L. Murray, Phase Diagrams of Binary Titanium Alloys, ASM International, Metals Park, Ohio, 1987.
[36] J. Robinson, B.A. Van Brussel, J.M. De Hosson, R.C. Reed, Mater. Sci. Eng., A 208 (1996) 143.
[37] C. Hu, H. Xin, L.M. Waston, T.N. Baker, Acta Mater. 45 (10) (1997) 4311.